Microporous and Mesoporous Materials 145 (2011) 41–50

Contents lists available at ScienceDirect

Microporous and Mesoporous Materials

journal homepage: www.elsevier.com/locate/micromeso

Characterization of dispersed indium species obtained by thermal treatment of In–NH_4-zeolites and their impact on the SCR of NO_x

Hernán P. Decolatti [a], Angel Martínez-Hernández [b], Laura B. Gutiérrez [a], Gustavo A. Fuentes [c], Juan M. Zamaro [a,*]

[a] Instituto de Investigaciones en Catálisis y Petroquímica, INCAPE (FIQ, UNL, CONICET), Santiago del Estero 2829, C.P. 3000, Santa Fe, Argentina
[b] Facultad de Ciencias Químicas, Universidad Autónoma de Nuevo León, C.P. 66400, N.L., Mexico
[c] Área de Ingeniería Química, Universidad A. Metropolitana – Iztapalapa, A.P. 55-534, 09340 México, D.F., Mexico

ARTICLE INFO

Article history:
Received 27 January 2011
Received in revised form 14 April 2011
Accepted 16 April 2011
Available online 23 April 2011

Keywords:
SCR of NO_x
Indium-zeolites
Dispersion
Impregnation
Exchange

ABSTRACT

Indium species dispersed on zeolites by high temperature treatment in air of indium-impregnated NH_4-zeolites were characterized and related to the catalytic behavior of the solids in the selective catalytic reduction of NO_x. NO-TPD, H_2-TPR and CO-TPR experimental results show that higher temperatures increase the fraction of dispersed InO^+ and In_xO_y phases. These species can oxidize nitric oxide to NO_2 and are in greater amounts on the mordenite framework. X-ray indium mapping and TEM observations show a heterogeneous distribution of In_2O_3 particles in solids with higher indium content. These oxides have smaller crystal size and a larger interaction in the framework of ZSM5. TGA–SDTA results point out that the thermal treatment simultaneously produces a solid-state indium exchange and a zeolite dehydroxylation, the exchange level being higher at larger indium contents. The catalytic behavior of the In–zeolites studied can be explained in terms of the type and proportion of indium species present according to the indium loading, thermal treatment and type of zeolite framework. For both zeolites, a higher temperature treatment extends the NO_x conversion windows because there are larger amounts of active InO^+. But the maximum deNO_x activity is lower for In–mordenite due to the larger amounts of In_xO_y in this zeolite. This non-selective phase increases the methane conversion level. When the indium content is higher, the deNO_x activity further increases, in line with a larger fraction of active InO^+ species. Besides, the catalytic activity of the solids does not decrease despite the excess of indium in these samples under the form of In_2O_3 crystals.

1. Introduction

One of the alternatives to control NO_x emissions is through their selective catalytic reduction with hydrocarbons in excess of oxygen using metal-zeolites [1,2]. The study of this type of catalysts developed along the last two decades since Armor et al. in a pioneering work, discovered that Co–ZSM5 can effectively reduce NO_x with methane in the presence of excess oxygen [3]. The same authors discovered later that other combinations such as Mn^{2+} and Ni^{2+} with certain types of zeolites, e.g., ZSM-5 and mordenite are active catalysts for this reaction [4]. However, among the many metal–zeolite combinations that have been explored since, those based on indium appear as one of the most promising because of their high catalytic activities for NO reduction when CH_4 is used as a reductant, mainly In–ZSM5, In–mordenite [5–12] and also In–Ferrierite [1,13]. Different methods have been developed to add indium to zeolites, which determine the type of dispersed indium phases [14]. Among the well-known methods for indium incorporation, we could mention the following techniques: reductive solid-state ion exchange (RSSIE) [15,8,12], ionic exchange from an indium salt solution [9,11,13], indium precipitation [8], sublimation and treatments of physical mixtures of zeolite and indium oxide [2,7,16], some of which are well described in the literature [8,14]. The method that has been most extensively studied is the RSSIE in which reductant and oxidative atmospheres with heating are alternated at high temperature to generate the exchanged active indium species. It has recently been shown that this process can also be carried out alternating atmospheres of argon and oxygen [17]. Indium-exchanged mordenites from In^0/H-mordenite mixtures have also been prepared through oxidative exchange procedures [18]. It should also be mentioned that several other studies have been published in which a second metal is added to In–zeolites in order to improve their catalytic performance [16,11,19].

A less commonly used variant of the indium SSIE is to perform the exchange by direct heating of indium-impregnated zeolites in an oxidant atmosphere. In this way, very active In–zeolite catalysts for the SCR of NO_x have been obtained [6,10,20]. This method is also

* Corresponding author. Tel./fax: +54 0342 4536861.
E-mail address: zamaro@fiq.unl.edu.ar (J.M. Zamaro).

1387-1811/$ - see front matter © 2011 Elsevier Inc. All rights reserved.
doi:10.1016/j.micromeso.2011.04.018

suitable to prepare active In–zeolite structured catalysts for the same reaction [21,22]. The preparation is simple, involves only one thermal treatment and does not require changes of atmospheres, in contrast to RSSIE. Moreover, direct heating of metal-impregnated zeolites could be more reproducible compared with methods based on treatments of physical mixtures of zeolite and indium oxide. The latter depends on the grinding process and particle characteristics. It has been shown that a high temperature treatment of indium impregnated H-forms of zeolites provokes that indium sesquioxide reacts in a solid state reaction with the zeolite protons [7,10,23]. In this exchange the oxidation state of In is cationic (+3); then the exchange between indium and zeolite protons occurs via an acid–base reaction [7]: $In_2O_3 + 2H^+Z^- \rightarrow 2(InO)^+Z^- + H_2O$ (Z^- denotes zeolitic exchange positions).

We have recently reported the surface and structural characterization of indium impregnated zeolites treated at high temperature in air [24]. The main conclusions were:

– Thermal treatment causes a partial dealumination of mordenite whereas ZSM5 is a more stable framework as shown by ^{29}Si and ^{27}Al NMR results.
– It was observed by FTIR that In–zeolites treated with nitric oxide formed NO_2 on the surface of the solids.
– XRD showed that in solids containing above 4 wt.% of indium, crystalline In_2O_3 is formed.
– XPS indicated the presence of two surface species with different interaction with the zeolite framework.

The aim of the present work is to study in greater depth the dispersion characteristics of indium species formed during high temperature treatments in air of indium-impregnated NH_4-zeolites, as well as their impact on the SCR of NO_x. We report on the effect of temperature treatment, indium loading and zeolite framework.

2. Experimental

2.1. In–zeolite preparation procedure

NH_4–mordenite Zeolyst (Si/Al = 10) and NH_4–ZSM5 Zeolyst (Si/Al = 15) were impregnated while stirring in an excess of indium solution (0.5 g l^{-1} of $In(NO_3)_3$ Aldrich P.A.). The resulting slurry was evaporated to dryness and maintained at 120 °C overnight. In this way, all indium incorporated to zeolites by the impregnation method (with an indium solution of known concentration) was exactly the same as the one that finally remained in the solids. Afterwards, a calcination step was carried out heating in synthetic air at 10 °C min^{-1} up to 500 °C and maintaining at this temperature for 12 h. Some aliquots of the indium-zeolite samples calcined at 500 °C were subject to a further calcination step at 700 °C by 2 h. In this way, different solids treated at 500 °C and 700 °C in air atmosphere were obtained with indium contents of 4 and 8 wt.% for both zeolites. For the samples with 8 wt.% of indium, the theoretical maximum degrees of exchange (as InO^+) were 47% and 68% for In(8)–mordenite and In(8)–ZSM5, respectively. By means of N_2 adsorption measurements, the obtained BET surface areas of the supports were 477 m^2/g for NH_4–mordenite and 380 m^2/g for NH_4–ZSM5 whereas for the samples containing 8 wt.% of indium, the BET surface areas were 351 m^2/g for In(8)–mordenite and 326 m^2/g for In(8)–ZSM5.

2.2. Characterization techniques

2.2.1. Temperature-programmed desorption of NO (NO-TPD)

The sample (50 mg) was heated in a He flow at 400 °C for 2 h in order to clean the surface. It was then cooled to r.t. in a flow of dry He and immediately afterwards put in contact with dry NO diluted in He (5000 ppm) for 20 min. Then, NO was purged from the gas phase and the programmed desorption was started at a heating rate of 10 °C min^{-1}, measuring the gas concentration (NO_x) at the outlet of the reactor with an FTIR instrument (Mattson Genesis II) equipped with an on-line cell with CaF_2 windows for gas phase analysis. The measurements were carried out taking successive spectra every two minutes during the temperature ramp.

2.2.2. Thermogravimetric analysis (TGA) and single differential thermal analysis (SDTA)

A Mettler Toledo STAR^e with a TGA/SDTA851^e module was employed. For the SDTA® analysis, the temperature difference was referred to an electronically generated signal that reproduced the thermal response of an inert sample. For pre-drying, a temperature ramp from 30 °C to 150 °C in N_2 flow (50 mL min^{-1}) was applied with a heating rate of 15 °C min^{-1}. After that, the experiment was run from 150 °C to 1000 °C at a heating rate of 10 °C min^{-1} in a flow of air (industrial grade; 30 mL min^{-1}) employing 15–20 mg of solid placed inside a 70 μL alumina crucible. After the experiment, the derivate of TGA (DTGA) was also obtained for the exact determination of the transition temperatures.

2.2.3. Temperature-programmed reduction with H_2 (H_2-TPR)

The H_2-TPR was performed in an Okhura TP-2002S instrument equipped with a TCD detector with tungsten filaments and a molecular sieve 5 Å trap. The sample (50 mg) was first pretreated in situ with N_2 for 30 min at 300 °C before the TPR experiments. After that, the sample was cooled at r.t. in N_2 flow and the TPR was run immediately in a 5% H_2–Ar stream (15 mL min^{-1}), heating at 10 °C min^{-1} up to the maximum treatment temperature.

2.2.4. Temperature-programmed reduction with CO (CO-TPR)

The experiments with CO were performed using a gas mixture consisting of 5% of CO in He balance. Thirty milligrams of sample were placed in a quartz reactor, whereas 15 mL min^{-1} flowed through the reactor during the entire test. The temperature was raised from r.t. up to 800 °C with a heating rate of 10 °C min^{-1}. The evolved CO_2 from the reduction of samples was captured with a trap made of $NaOH/SiO_2$ located at the reactor outlet.

2.2.5. Transmission electron microscopy (TEM)

Specimen preparation was done by making a suspension of the powder sample in acetone that was ultrasonically dispersed. Some drops of this suspension were placed in a carbon-coated copper grid. TEM images were obtained with a JEOL-2000 FXII instrument with 0.28 nm point to point spatial resolution, operated at 200 keV.

2.2.6. X-ray microanalysis and elemental mapping

An X-ray microanalyzer Energy 300 coupled to a scanning electron microscopy JEOL JSM 6400 was employed. The analyses were performed on broad areas to get the elemental composition of the samples and in smaller selected areas on particles to perform elemental mapping. Samples were first dispersed in acetone and then put into a holder and covered with a thin film of graphite.

2.3. Catalytic evaluations

Catalysts were evaluated in a continuous flow system equipped with mass flow control-meters in the selective catalytic reduction (SCR) of NO_x with methane. The composition of the reacting stream was 1000 ppm NO, 1000 ppm CH_4, 10% O_2 in He balance. The reaction was performed at atmospheric pressure in a quartz reactor heated in a furnace with temperature controller. The temperatures ranged between 300 °C and 600 °C with a flow/catalyst weight ratio (F/W) of 500 mL min^{-1} g of $zeolite^{-1}$ (100 mg catalyst with a flow of

50 mL min^{-1} was employed) that means a space velocity (GHSV) of 15,000 h^{-1}. The sample was first heated in He up to 300 °C and then maintained 2 h to clean the catalyst and then, the reactant stream was fed and catalytic experiments in SCR of NO_x were performed. NO_x and CH_4 conversions were calculated as: $X_{NO_x} = \frac{2[N_2]}{[NO_x]^0} \times 100$ and $X_{CH_4} = \frac{[CH_4]^0 - [CH_4]}{[CH_4]^0} \times 100$, respectively, where X is conversion, $[NO_x]^0$ and $[CH_4]^0$ are inlet gas concentrations and $[N_2]$ and $[CH_4]$ are outlet gas concentrations in ppm. The analyses of gas composition in catalytic experiments were performed with a Shimadzu GC-2014 gas chromatograph equipped with a thermal conductivity detector (TCD) and a zeolite 5 Å column. Helium was used as carrier gas.

3. Results and discussion

3.1. Temperature-programmed desorption of NO (NO-TPD)

It has been recognized that on In–zeolites prepared by several different methods three main species could be present, namely, exchanged InO^+, In_2O_3 oxides and dispersed non-stoichiometric oxides like In_xO_y, the first one being the active site [7,10,12,13]. In all analyzed In-zeolite samples three NO-TPD signals were observed. Interestingly, NO_2 is the main gas evolved with a desorption taking place in two temperature zones. A signal of NO is also present at low temperature. The NO_x species observed in the NO-TPD runs were only NO and NO_2. The NO-TPD experimental results obtained for In(4)–mordenite and In(4)–ZSM5 are shown in Fig. 1. In view of the fact that the adsorbed gas was NO, it is likely that the NO_2 desorption originated from the NO oxidation caused by indium species. Moreover, the formation of NO_2 occurred at the surface of the solids and not in the gas phase, as confirmed by FTIR measurements of these same solids in which a NO_2 absorption band was identified [24]. The redox behavior of InO^+ species was observed in recent studies of Mihályi and Beyer [25] who found an interconversion between In^+ and $(InO)^+$ through FTIR measurements of adsorbed pyridine on In–zeolites. The oxidation of NO to NO_2 was also observed on other indium-exchanged zeolites, forming adsorbed (ONO)–InO^+ or NO_2–InO^+ species [26]. Then, the observed NO_2 desorption in our samples should be from NO oxidized on dispersed indium species, such as exchanged $(InO)^+$ and also probably on other highly dispersed oxides as In_xO_y.

Table 1 summarizes the NO-TPD results for the In–zeolites studied, showing the ratios between integrated areas under the peaks. It can be observed that there are changes in the relative amount of the total NO_2 evolved as a function of the different indium loadings (NO_2^{T700}/NO_2^{T500}). Moreover, for In–mordenite the ratio between the low and high temperature NO_2 peaks (NO_2^L/NO_2^H) changes (low temperature peaks are those in which the maximum lies between 70–110 °C, whereas high temperature peaks are those in which the maximum lies between 350–400 °C). The NO_2^L peak increases with respect to NO_2^H as a result of the higher temperature treatment while for higher loaded sample this ratio is smaller (Table 1). An increase in NO desorption is also observed with higher temperature treatments and indium loadings (NO^{700}/NO^{500}). Table 1 also shows that on the ZSM5 framework, the amount of desorbed NO_2 is lower than for the mordenite samples and that the higher temperature treatments do not substantially change the NO_2^L/NO_2^H ratio for this zeolite. All these observations demonstrate that NO-TPD is a sensitive technique to get information about the dispersion

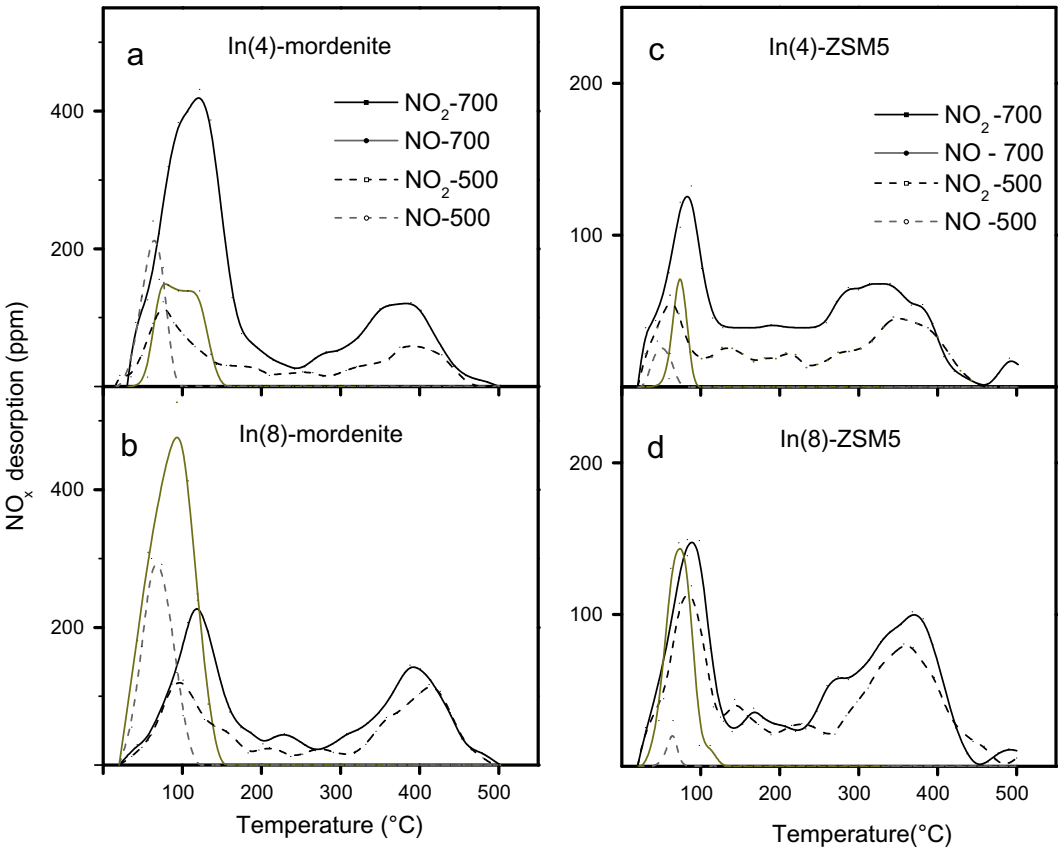

Fig. 1. NO-TPD profiles of In–zeolite solids: (a) In(4)–mordenite; (b) In(8)–mordenite; (c) In(4)–ZSM5; and (d) In(8)–ZSM5. Catalyst treated at 500 °C in dashed lines: NO_2 (dashed black); NO (dashed dark yellow). Catalyst treated at 700 °C in solid lines: NO_2 (solid black); NO (solid dark yellow). (For interpretation of the references to colour in this figure legend, the reader is referred to the web version of this article.)

Table 1
Relationships between NO-TPD signals of In–zeolites.

NOx ratios (ppm/ppm)	In–mordenite				In-ZSM5			
	4wt% In		8wt% In		4wt% In		8wt% In	
	500 °C	700 °C	500 °C	700 °C	500 °C	700 °C	500 °C	700 °C
[a] NO_2^L/NO_2^H	1.35	2.53	0.88	1.29	0.72	0.81	0.91	0.88
[b] $NO_2^{T\ 700}/NO_2^{T\ 500}$	3.21		1.55		1.92		1.25	
[c] $NO700/NO^{500}$	1.32		2.40		2.05		9.75	

[a] Ratio between the area of NO_2 peak desorbed at low temperature (NO_2^L) and the area of NO_2 peak desorbed at high temperature (NO_2^H). The low temperature peaks are those in which the maximum of the signals lies between 70–110 °C, whereas high temperature peaks are those in which the maximum of the signals lies between 350–400 °C.
[b] Ratio between the total amount of NO_2 desorbed from the sample treated at 700 °C (NO_2^{T700}) and total amount of NO_2 desorbed from the sample treated at 500 °C (NO_2^{T500}).
[c] Ratio between the NO desorbed from the sample treated at 700 °C (NO^{700}) and the NO desorbed from sample treated at 500 °C (NO^{500}).

of indium species present in the zeolites and that the NO_2 signals are related to the more dispersed species while the NO signals are related to the less dispersed ones. NO_2 formation matches the total amount of dispersed phases while the NO_2^L/NO_2^H matches the proportion of the possible species involved; exchanged InO^+ and dispersed In_xO_y. The desorption of NO is linked to the larger In_2O_3 particles that cannot oxidize adsorbed NO. The observations indicate that higher temperature treatment and indium content in the zeolites increase the amount of both the highly dispersed InO^+ and In_xO_y but also the low dispersed In_2O_3 phases. These variations in the proportion of indium species formed will be further corroborated in the next discussion of TPR characterization.

3.2. Temperature-programmed reduction with H_2 (H_2-TPR)

TPR profiles of In–mordenite show two main peaks in the 200–400 °C range as observed in Fig. 2a. For all mordenite samples, the peak at low temperature increases after treatment at 700 °C. For the sample with higher indium content and treated at 500 °C, the intensity of the 350 °C reduction peak increases compared with the low loading sample, and the profile shows a tail towards higher temperatures. When this sample is further treated at 700 °C, a new peak at 750 °C appears and there is also an increase of the low temperature peaks as shown in Fig. 2a. To assign these signals, we rely on previous H_2-TPR studies. For In–mordenite obtained trough the RSSIE method [18,27], it has been proposed that the 350 °C H_2-TPR signal is caused by the reductive exchange of In_2O_3 with the zeolite as: $In_2O_3 + 2H_2 + 2H^+Z^- \rightarrow 2In^+Z^- + H_2O$. If this sample is later oxidized, $(InO)^+Z^-$ is produced and a subsequent TPR shows a signal shifted to lower temperature (250 °C) according to: $(InO)^+Z^- + H_2 \rightarrow In^+Z^- + H_2O$. By comparing these assignments with the reduction profiles of our samples, the low temperature peaks can be attributed to easily reducible dispersed indium phases such as $(InO)^+$ and In_xO_y whereas. The higher temperature peak is ascribed to the reduction of bulk In_2O_3 phases to form In^+Z as already observed in other indium-loaded zeolites [23]. The H_2-TPR profiles of In–mordenite follow the tendency observed in NO-TPD experiments for samples with different indium content and thermal treatment; the highly dispersed species increases with high temperature treatment while the less dispersed one increases with the indium content.

The H_2-TPR curves of In–ZSM5 samples (Fig. 2b) also show peaks in the 200–450 °C range. The In(4)–ZSM5-500 sample has a small proportion of low dispersed phases (shoulder near

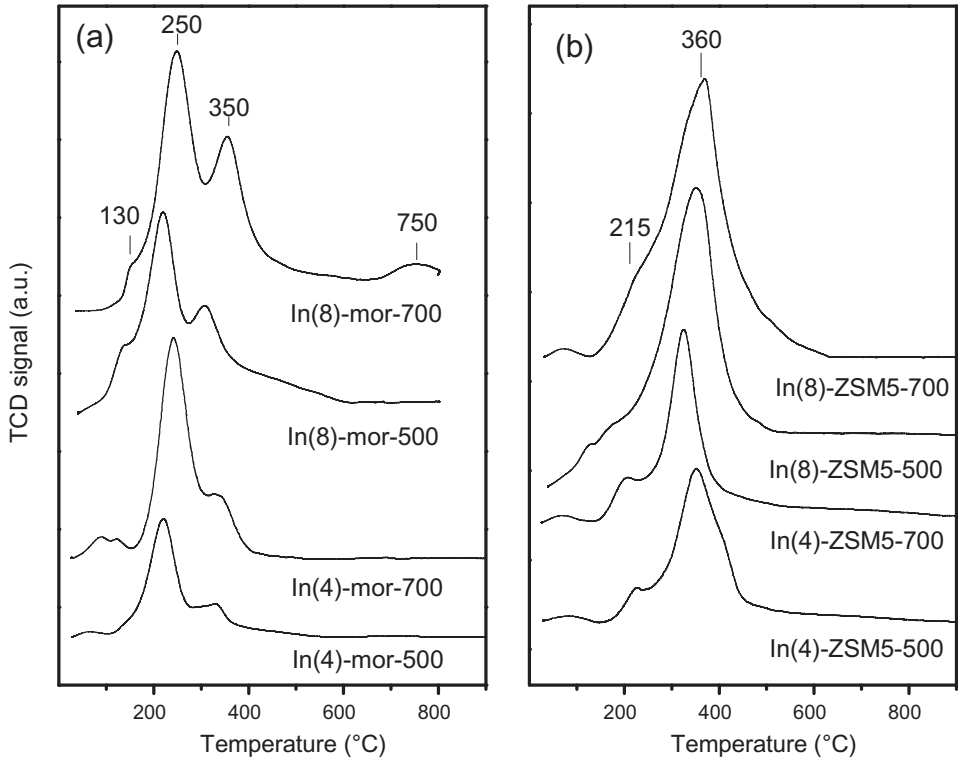

Fig. 2. Temperature-programmed reduction with hydrogen (H_2-TPR): (a) In–mordenite samples; (b) In–ZSM5 samples.

450 °C) but increases after the 700 °C treatment, as evidenced by the disappearance of the shoulder and the increment of the low temperature peaks. For the large loaded sample, the TPR peaks are more intense but broader indicating a higher amount of dispersed phases and with a wider degree of interaction, respectively. The higher temperature reduction peak ascribed to bulk In_2O_3 was not observed. However, the presence of crystalline In_2O_3 in this sample has been probed by XRD analysis [24]. Therefore, these indium crystals should be in higher interaction with this zeolite and correspond to the tail of TPR profile signal above 400 °C (see TPR of In(8)–ZSM5-700 in Fig. 2b).

Unlike H_2-TPR, the reduction with carbon monoxide could differentiate between reducible oxygenated species that reinforce the above discussed results. Next we present the CO-TPR characterizations of In–zeolites.

3.3. Temperature-programmed reduction with CO (CO-TPR)

The reduction of indium oxides by CO could only be caused by abstraction of oxygen atoms available in these species, thus forming CO_2. The capacity of indium oxides to lose oxygen atoms has been shown in the previously discussed NO-TPD experiments. In Fig. 3, the CO-TPR of In–ZSM5 and In–mordenite are presented. As expected all curves are shifted to higher reduction temperatures (above 400 °C), compared to the respective H_2-TPR, because CO is a weaker reducing agent than H_2. For In–mordenite (Fig. 3a), the 700 °C treatment produces an increment of the signals with a displacement towards higher temperatures. In one of the few CO-TPR studies of In–mordenite, Schütze et al. [27] found a broad signal between 250–600 °C that they assigned to oxo-cations species, such as $(InO)^+$. In view of our previously discussed NO-TPD and H_2-TPR results, these shifts should be associated with the development of indium oxygenated dispersed phases while the changes in the low temperature range should be caused by indium oxides with low dispersion, i.e. In_2O_3 crystals.

On the other hand, for In–ZSM5 samples we observed trends of CO-TPR similar to those of In–mordenite (Fig. 3b). The dispersed phases increased with higher temperature treatments and also further increased with higher indium loadings. However, on higher loaded samples negative peaks appeared due to a CO adsorption that was released during the TPR experiment (Fig. 3b). As CO adsorption was not observed for In(8)–mordenite, it can then be inferred that the low dispersed In_2O_3 particles formed on In(8)–ZSM5 are responsible for the observed CO adsorption in that case. It is known that In_2O_3 nanoparticles are sensitive to adsorb CO [28] but to a different degree depending on particle size and shape, compared with In_2O_3 particles that do not interact with CO. As shown in previous H_2-TPR experiments, there are differences between the In_2O_3 crystals present in mordenite and ZSM5, most likely due to the fact that crystal size produced different interactions with the zeolite matrix. To further confirm this assumption, TEM observations were performed.

3.4. Transmission electron microscopy

Fig. 4 shows TEM images of In–mordenite and In–ZSM5 samples. In the In(8)–mordenite sample (Fig. 4a and b) there appear a large number of islands as dark spots spread on the surface of zeolite crystals. These particles are ascribed to indium oxide and have a size in the 4 nm to 10 nm range. In the In(8)–ZSM5 sample (Fig. 4c and d), segregated particles are also observed. However, their size is much smaller compared to that in mordenite. The detected particles are smaller than 3 nm and are aligned along the edges of the zeolite crystals, probably due to the accumulation of precursors in the intercrystalline voids. The presence of larger In_2O_3 particles on In(8)–mordenite agrees with the H_2-TPR of this sample, which showed a reduction peak of oxide species with a bulk behavior. The smaller particle size of In_2O_3 on In(8)–ZSM5 is consistent with the higher interaction of the oxide in this zeolite, which was also observed in H_2-TPR experiments (tail above

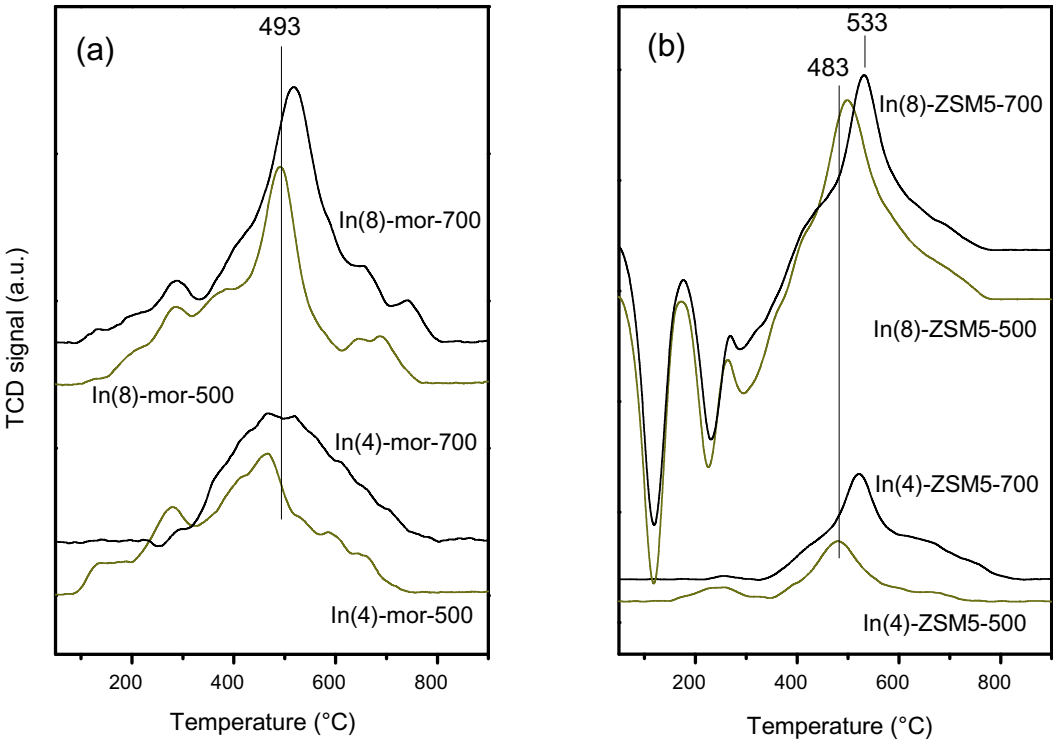

Fig. 3. Temperature-programmed reduction with carbon monoxide (CO-TPR): (a) In(4)–mordenite and In(8)–mordenite; (b) In(4)–ZSM5 and In(8)–ZSM5. Figure shows curves for samples treated at 500 °C and samples treated at 700 °C.

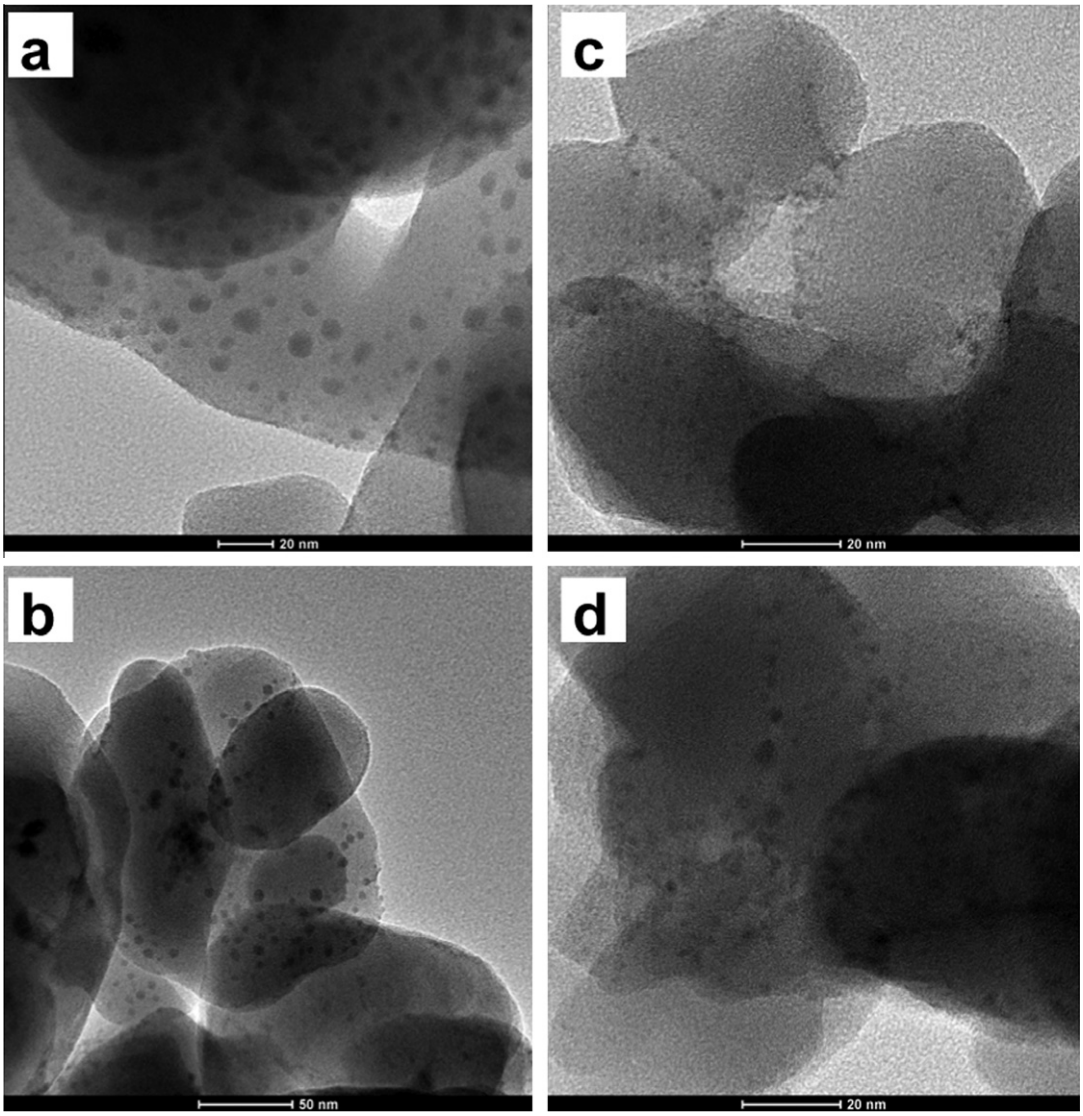

Fig. 4. Transmission electron microscopy (TEM) images: (a) and (b) In(8)–ZSM5 sample treated at 700 °C; (c and d) In(8)–mordenite sample treated at 700 °C.

450 °C). No dispersed oxides were detected by TEM in the samples containing 4 wt.% indium. The different particle size of In_2O_3 in the catalysts with high indium loading could lead to a different interaction with the zeolite, deriving in a different CO adsorption behavior such as the one observed in CO-TPR for both zeolite samples.

3.5. X-ray microanalysis and indium elemental mapping

The observation of the higher indium loaded zeolites by SEM in backscattering electron mode shows some bright areas in zeolite particles as shown in Fig. 5a and b. The increased density of electrons in these sectors is due to the higher backscattered electrons because of the heavier indium atoms. Actually, local X-ray analysis of indium in those areas showed a higher concentration of indium atoms as the one indicated in the legend of Fig. 5. The circles drawn indicate the approximate area of interaction during the analysis. Fig. 5c shows the X-ray indium mapping of In(8)–ZSM5 in which it is clearly seen that higher indium concentration matches with the zones of higher backscattered electrons in the image of Fig. 5b. The indium oxide particles segregated on zeolite crystals, as observed by TEM, originate a non-uniform distribution of indium in the catalyst. It should be mentioned that X-ray indium mapping on 4 wt.% In loaded samples did not show inhomogeneities in indium distribution.

3.6. Thermogravimetric analysis (TGA) and single differential thermal analysis (SDTA)

The indium impregnated zeolites, should exhibit changes in mass and thermal response during the thermal treatment of impregnated solids. We performed TGA-SDTA experiments trying to follow these changes. TGA of NH_4–mordenite (Fig. 6a) shows a weight loss at low temperature due to water release followed by another process that starts near 350 °C associated with NH_3 evolution (total weight loss at low temperature of 10.5 wt.%), whereas another one after 600 °C was caused by dehydroxylation. These are the main processes that are likely to occur in the ammonium-zeolite. The SDTA curve shows endothermal processes at the same temperatures, in agreement with the said processes. However, STDA shows two peaks in the high temperature zone in agreement with a dehydroxylation of OH in two environments for this zeolite. FTIR studies of this support showed two components in the 3600 cm^{-1} region due to the stretching vibration of

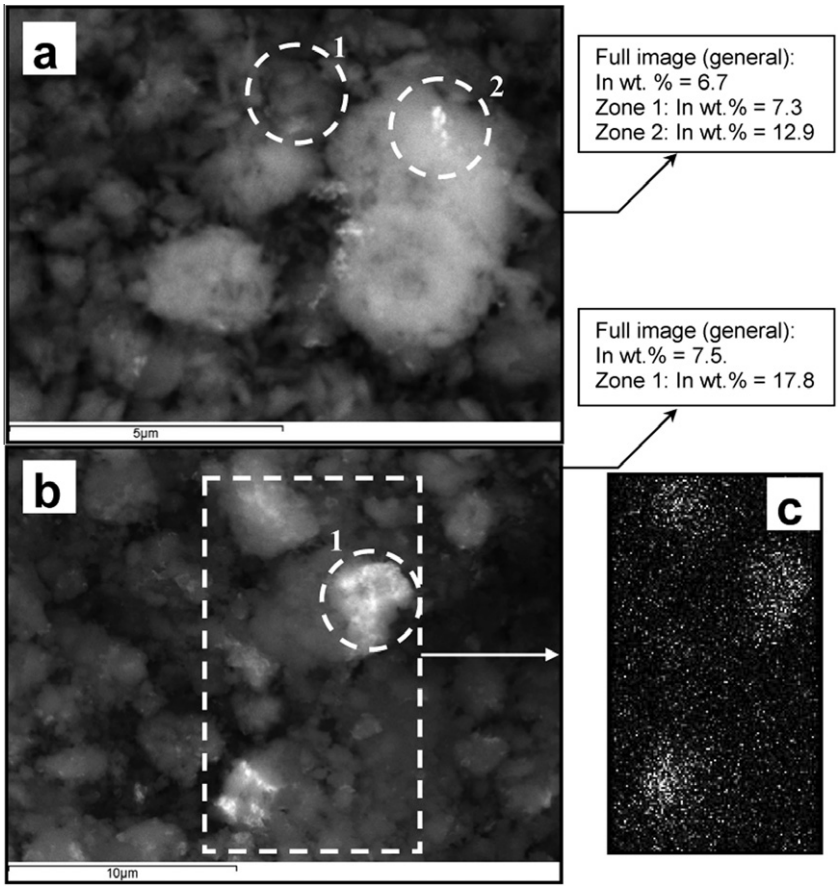

Fig. 5. Backscattering electron images and X-ray indium analysis: (a) Backscattering image of In(8)–mordenite-700; (b) backscattering image of In(8)–ZSM5-700. (c) X-ray indium mapping on sector indicated in (b) (in circles, zones of punctual X-ray analyses are indicated).

different acidic OH [24,29]. For the NH_4–ZSM5 zeolite there is also a weight loss at low temperatures due to H_2O and NH_3 (total weight loss at low temperature of 6.4 wt.%) and another weight loss starting near 600 °C due to thermal dehydroxylation (Fig. 6c). However, the STDA profile in the high temperature zone showed only one big endothermic peak that is centered at 850 °C.

For the analysis of the TGA-SDTA curves, only the changes that appear after 600 °C will be of interest for the following discussion. Table 2 summarizes the normalized mass loss and SDTA relationships for both NH_4-zeolites and In–zeolites above 600 °C. It can be seen that the thermal treatment originates a smaller mass loss at temperatures above 600 °C in NH_4–ZSM5 than in NH_4–mordenite (relationship of 0.46), which is indicative of a lower magnitude of dehydroxylation in the former. However, as shown in Table 2 the ratios between the integrated areas of normalized SDTA signals at temperatures above 600 °C, have opposite trends (relationship of 1.55). In view of the fact that the SDTA signal is proportional to mass and ΔH involved in the processes, the said ratio represents differences in ΔH of the dehydroxylation between both zeolites. The higher magnitude of dehydroxylation in NH_4–mordenite, albeit with lower energies (ΔH) compared to NH_4–ZSM5, is consistent with the greater amount of OH groups present in that zeolite and its lower thermal stability [24]. These variables are of relevance on solid-state indium exchange processes.

In indium-impregnated samples, the TGA curves show a bigger weight loss at low temperatures as shown in Fig. 6 for In(4)–mordenite and In(4)–ZSM5, due to a release of water, ammonium and nitrate incorporated during the impregnation step (total weight loss at low temperature of 13.2 wt.% and 9.5 wt.%, respectively). For the 8 wt.% indium samples, the corresponding total weight loss at low temperature was 15.4 wt.% for In(8)–mordenite and 11.2 wt.% for In(8)–ZSM5. Differences in SDTA signals above 600 °C of In–zeolites are noticed. For In(4)–mordenite (Fig. 6b) a single broad endothermic signal with higher intensity than NH_4–mordenite is observed and for In(8)–mordenite, this signal further increases but this increment is not proportional to the indium content as shown in Table 2. This result suggests that two processes with different energies could be taking place, as indium exchange reactions occurring at the two OH sites present in this zeolite. The bridging OH groups in mordenite have been assigned to OH located in the side pockets and that located in the main channels, the former having a higher acidity [29]. The different reactivity of bridging OH groups (exchange sites) in this zeolite was also reported for cobalt-exchanged mordenite [30]. The increased SDTA signals with indium loading correspond to a higher indium exchange level. The exchange probably takes place first with more reactive (acid) sites and then continue with the less acidic OH.

For In–ZSM5 solids (Fig. 6d), the SDTA analysis above 600 °C shows a single and broad endothermic signal that increases proportionally with the indium content (Table 2). This implies indistinguishable reactive sites during the SSIE. The similarity of acidic OH in H–ZSM5 (exchange sites) has been determined by spectroscopic analysis because of the similar chemical environment of the bridging OH in this zeolite [31], supporting the SDTA observations.

From the above results, it can be inferred that in both indium-impregnated NH_4-zeolites, thermal treatment in air causes indium solid-state exchange simultaneously to thermal dehydroxylation of

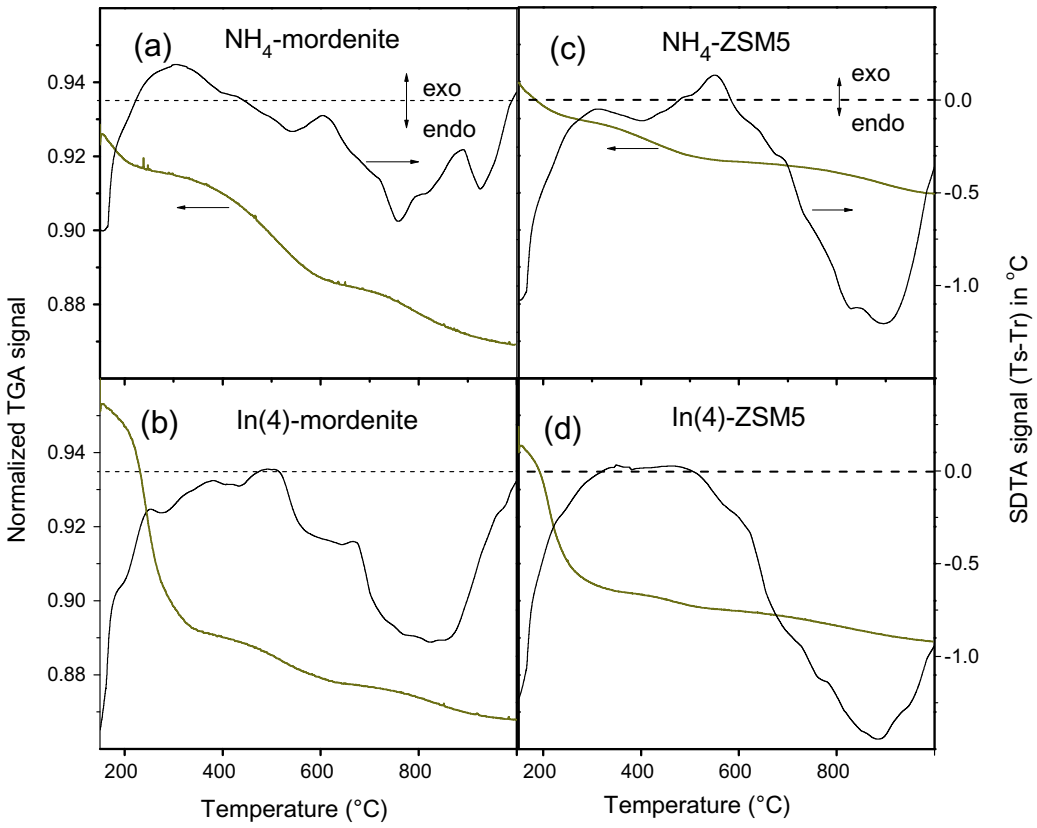

Fig. 6. Thermogravimetric (TGA) and single differential thermal analysis (SDTA): (a) NH_4–mordenite; (b) In(4)–mordenite. (c) NH_4–ZSM5; (d) In(4)–ZSM5.

Table 2
Relationships between SDTA and TGA signals above 600 °C for ammonium supports and In–zeolites.

Indium content (wt.%)	TGANH4-ZSM5/NH4-mordenite[a]	SDTANH4-ZSM5/NH4-mordenite[b]	SDTAIn–mordenite/NH4-mordenite[c]	SDTAIn-ZSM5/NH4-ZSM5[c]
0	0.46	1.55	1	1
4	-	-	1.38	1.30
8	-	-	2.35	1.62

[a] Ratio between mass loss of the ammonium-supports from 600 °C to 1000 °C. The mass loss of each support was first normalized with respect to their mass at 600 °C.
[b] Ratio between the integrated areas of SDTA signals of the supports from 600 °C to 1000 °C. The SDTA signals for each support were first normalized with respect to their mass at 600 °C.
[c] Ratio between the integrated areas of the SDTA signals of In-zeolite and support from 600 °C to 1000 °C. The SDTA signals for each sample were first normalized with respect to their mass at 600 °C.

the zeolites, the former being more energetic and occurring probably in two events on In–mordenite, each event corresponding to different acidic OH sites.

3.7. Catalytic evaluations

Fig. 7 shows the catalytic features of In–mordenite and In–ZSM5 solids in the SCR of NO_x. For both types of zeolite supports, the catalysts treated at 700 °C have higher NO_x conversion than those treated at 500 °C. Since it has been well established that exchanged $(InO)^+$ is the main active site for the said reaction [7,10,20], the observed trend is in line with the increase in the amount of this species with higher temperature treatments. As a matter of fact, the NO-TPD and TPR experiments indicated an increase of the concentration of highly-dispersed indium species in samples treated at 700 °C. The amounts of these species were higher for In–mordenite; however it can be seen that the maximum NO_x conversion level for this In-zeolite is lower than that obtained with In–ZSM5 (Fig. 7). This fact indicates that other indium species must be influencing the catalytic performance.

The SCR of NO_x reaction is a sum of three main reactions: the oxidation of NO to NO_2; the reaction between NO_x and the hydrocarbon to give N_2 and CO_x (selective reaction); and the reaction of the hydrocarbon with oxygen (non-selective reaction). The more active the catalyst for the non-selective reaction, the lower NO_x conversion is obtained due to a lower availability of hydrocarbon. By comparing curves in Fig. 7 it can be clearly seen that In–mordenite is more active for methane combustion than In-ZSM5, thus explaining the lower activity of the former for NO_x reduction. Furthermore, 100% of CH_4 conversion is reached for In(4)–mordenite samples at 500 °C (Fig. 7c), but only 57–67% of CH_4 conversion is reached at the same temperature in the case of In(4)–ZSM5 (Fig. 7a). The high activity for the non-selective reaction in In–mordenite should be related to the formation of non-selective indium species in this zeolite framework. As regards these species, characterizations indicate that there are higher amounts of dispersed In_xO_y in mordenite. These species should be responsible for the lower selectivity and activity on the In–mordenite catalysts.

When indium content is higher in both zeolites, dispersed indium species are still present and in higher proportions as

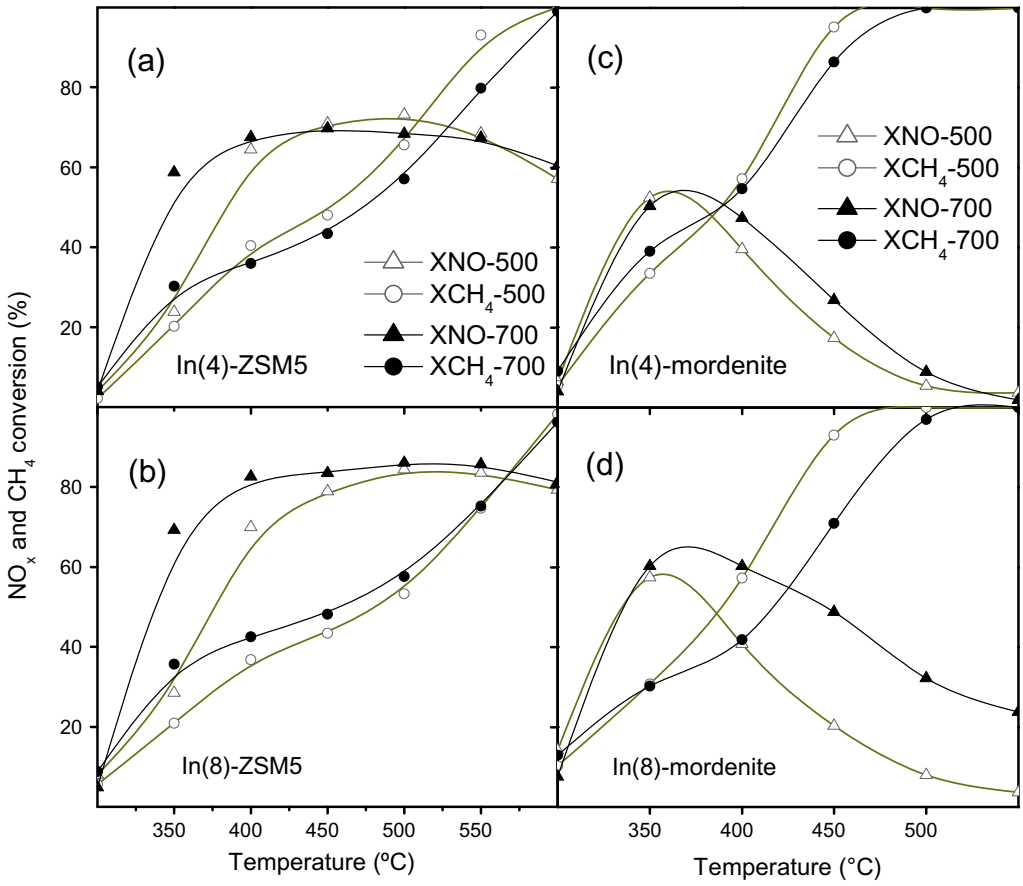

Fig. 7. Catalytic features of thermally treated indium-impregnated NH_4-zeolites in the SCR of NO_x with methane in oxygen excess. NO_x and CH_4 conversions curves for: (a) In(4)–ZSM5; (b) In(8)–ZSM5; (c) In(4)–mordenite; (d) In(8)–mordenite. Figure shows curves for samples treated at 500 °C and samples treated at 700 °C (the conditions in SCR of NO_x were GHSV 15,000 h^{-1}; 1000 ppm of CH_4 and NO, 2% O_2 in He balance).

observed by NO-TPD and TPR characterizations. In In(8)–ZSM5, the activity is higher than in 4 wt.% In loaded samples (Fig. 7d) in agreement with higher amounts of active InO^+ sites. The activity level also shows that the indium excess produced in this zeolite as low dispersed oxides, as shown by TPR and TEM, is not detrimental to the catalyst activity. Then, they should not significantly block the accessibility of reagents to active sites in contrast to other cases [6]. It can be seen that the 700 °C treatment extends the windows of high NO_x conversion for both zeolites. In In–mordenite it does so towards higher temperatures whereas in In–ZSM5, towards the lower temperature range. In the case of high metal loaded samples, the activity increase with the higher temperature treatment can be ascribed not only to higher amounts of InO^+ but also to the decrease of non-selective In_xO_y phases that can sinter forming In_2O_3 as above discussed. This situation is clear for In(8)–mordenite (Fig. 7d) in which a decrease of methane conversion together with the increase of deNO_x activity level above 350 °C result in a significant increase of the selectivity to the SRC reaction.

4. Conclusions

The dispersion of indium species on indium-impregnated NH_4–mordenite and NH_4–ZSM5 caused by thermal treatments in air atmosphere was characterized and related to their activities in the SCR of NO_x. A treatment at 500 °C produces the exchanged InO^+ species in both zeolites and also other highly dispersed In_xO_y phases. Both can oxidize NO to NO_2 at two different temperatures as shown by NO-TPD experiments (Fig. 1). A further treatment at 700 °C increases the amount of dispersed and highly reducible phases as shown by TPR (Figs. 1 and 2). In the case of samples with higher indium loadings, the amount of both dispersed phases and the less dispersed In_2O_3 also increases (Figs. 1–3). As shown by TEM, these oxide particles have a size of about 4–10 nm in mordenite and less than 3 nm in ZSM5, which has a higher interaction with the latter (Fig. 4). This particle oxide segregation produces a non-homogeneous distribution of indium on zeolite crystals as shown by the backscattering electron images and X-ray indium mapping analysis (Fig. 5). The thermal treatment of impregnated solids involves endothermic reactions at temperatures above 600 °C as shown by SDTA, due to the simultaneous thermal dehydroxylation and solid-state indium exchange processes. SDTA also shows that the indium exchange level increases with the indium content (Fig. 6). The catalytic activity of the In–zeolites changes depending on the proportion of indium species in the material, a function of indium loading, thermal treatment and zeolite framework (Fig. 7). Solids treated at 500 °C are active for the SCR of NO_x due to the partial exchange of InO^+. Both In–zeolites treated at higher temperature increase the solid-state reaction level, provoking an enhancement in NO_x conversion. However, the larger amount of In_xO_y on In–mordenite is responsible for the lower activity of this catalyst because these species are more active for methane combustion. Higher contents of indium further improve the NO_x conversion in both zeolites in line with the generation of new InO^+ sites and due to the sintering of non-selective In_xO_y phases forming In_2O_3. This segregated In_2O_3 has no detrimental effect on the catalytic activity.

Acknowledgements

The authors are grateful for the financial support received from CONICET and ANPCyT from Argentina, CONACYT and UAM Iztapalapa from Mexico and Project CIAM. Thanks are also given to Dr. Eduardo Miró for his collaboration and to Prof. Elsa Grimaldi for the English language editing.

References

[1] Y. Traa, B. Burger, J. Weitkamp, Microporous Mesoporous Mater. 30 (1999) 3.
[2] A. Kubacka, J. Janas, E. Wloch, B. Sulikowski, Catal. Today 101 (2005) 139.
[3] Y. Li, J.N. Armor, Appl. Catal. B: Environ. 1 (4) (1992) L31.
[4] Y. Li, J.N. Armor, Appl. Catal. B: Environ. 2 (2–3) (1993) 239.
[5] E. Kikuchi, M. Ogura, Catal. Surv. Jpn. 1 (1997) 227.
[6] X. Zhou, T. Zhang, Z. Xu, L. Lin, Catal. Lett. 40 (1996) 35.
[7] E. Kikuchi, M. Ogura, I. Terasaki, Y. Goto, J. Catal. 161 (1996) 465.
[8] T. Sowade, C. Schmidt, F.W. Schütze, H. Berndt, W. Grünert, J. Catal. 214 (2003) 100.
[9] M. Ogura, M. Hayashi, E. Kikuchi, Catal. Today 42 (1998) 159.
[10] E.E. Miró, L. Gutiérrez, J.M. Ramallo-López, F.G. Requejo, J. Catal. 188 (1999) 375.
[11] A. Kubacka, J. Janas, B. Sulikowski, Appl. Catal. B 69 (2006) 43.
[12] M. Ogura, T. Ohsaki, E. Kikuchi, Microporous Mesoporous Mater. 21 (1998) 533.
[13] J.M. Ramallo-López, F.G. Requejo, L.B. Gutierrez, E.E. Miró, Appl. Catal. B. Environ. 29 (2001) 35.
[14] C. Schmidt, T. Sowade, E. Loffler, A. Birkner, W. Grunert, J. Phys. Chem. B 106 (2002) 4085.
[15] H.K. Beyer, R.M. Mihályi, Ch. Minchev, Y. Neinska, V. Kanazirev, Microporous Mater. 7 (1996) 341.
[16] F. Lónyi, H.E. Solt, J. Vaylon, H. Decolatti, L.B. Gutierrez, E.E. Miró, Appl. Catal. B. Environ. 100 (2011) 133.
[17] R.M. Mihályi, Z. Schay, Á. Szegedi, Catal. Today 143 (2009) 253.
[18] H. Solt, F. Lónyi, R.M. Mihályi, J. Valyon, L.B. Gutiérrez, E.E. Miró, J. Phys. Chem. 112 (2008) 19423.
[19] R. Serra, M.J. Vecchietti, E. Miró, A. Boix, Catal. Today 133 (2008) 480.
[20] J.M. Ramallo-López, L.B. Gutierrez, A.G. Bibiloni, F.G. Requejo, E.E. Miró, Catal. Lett. 82 (2002) 131.
[21] J.M. Zamaro, M.A. Ulla, E.E. Miró, Chem. Eng. J. 106 (2005) 25.
[22] J.M. Zamaro, M.A. Ulla, E.E. Miró, Appl. Catal. A 308 (2006) 161.
[23] X. Zhou, Z. Xu, T. Zhang, L. Lin, J. Mol. Catal. A: Chem. 122 (1997) 125.
[24] J.M. Zamaro, E.E. Miró, A.V. Boix, A. Martínez-Hernández, G.A. Fuentes, Microporous Mesoporous Mater. 129 (2010) 74.
[25] M.R. Mihályi, H.K. Beyer, Chem. Commun. (2001) 2242.
[26] A.N. Beltramone, L.B. Pierella, F.G. Requejo, O.A. Anunziata, Catal. Lett. 91 (2003) 19.
[27] F.W. Schütze, H. Berndt, M. Ritcher, B. Lücke, C. Schmidt, T. Sowade, W. Grünert, Stud. Surf. Sci. Catal. 135 (2001) 135.
[28] M.I. Baraton, L. Merhari, H. Ferkel, J.F. Castagnet, Mater. Sci. Eng. C 19 (2002) 315.
[29] V.L. Zholobenko, M.A. Makarova, J. Dwyer, J. Phys. Chem. 97 (1993) 5962.
[30] L.B. Gutierrez, E.E. Miró, M.A. Ulla, Appl. Catal. A: Gen. 321 (2007) 7.
[31] D. Kaucký, A. Vondrová, J. Dedecek, B. Wichterlová, J. Catal. 194 (2000) 318.